frontiers | Frontiers in Physics

TYPE Original Research
PUBLISHED 23 September 2022
DOI 10.3389/fphy.2022.1028856

OPEN ACCESS

EDITED BY
Yufei Ma,
Harbin Institute of Technology, China

REVIEWED BY
Jin Li,
Northeastern University, China
Qiang Liu,
Northeastern University at Qinhuangdao, China

*CORRESPONDENCE
Zhiying Liu,
zyingliu@163.com

SPECIALTY SECTION
This article was submitted to Optics and Photonics, a section of the journal Frontiers in Physics

RECEIVED 26 August 2022
ACCEPTED 05 September 2022
PUBLISHED 23 September 2022

CITATION
Liu Z, Li H and Zhang Z (2022), Sagnac ring and photonic crystal fiber structure refractive index sensor with high birefringence and low temperature sensitivity.
Front. Phys. 10:1028856.
doi: 10.3389/fphy.2022.1028856

Sagnac ring and photonic crystal fiber structure refractive index sensor with high birefringence and low temperature sensitivity

Zhiying Liu[1]*, Hao Li[1] and Zhiwen Zhang[2]

[1]School of Opto-Electronic Engineering, Changchun University of Science and Technology, Changchun, China, [2]Heilongjiang Province Key Laboratory of Laser Spectroscopy Technology and Application, Harbin University of Science and Technology, Harbin, China

In this paper, a novel refractive index sensor based on photonic crystal fiber and Sagnac ring is studied. The sensor adopts Mach-Zehnder interference principle. The production and experimental steps are as follows: The first step is to fuse the single-mode fiber with the photonic crystal fiber to form a basic sensing unit. The second part uses the coupling birefringence effect of the tapered coupler to fold and fuse the single-mode fiber together to form the Sagnac interferometer. Through this structure, the sensor has the characteristics similar to the polished photonic crystal fiber sensor, while the fabrication complexity is greatly reduced. The refractive index sensing capability and temperature stability of the two structures are analyzed experimentally. Simulation results show that the structure has high birefringence effect. Experimental results show that the proposed photonic crystal fiber combined with Sagnac ring sensor has good sensing performance in the refractive index range of 1.3355–1.3560. Compared with the sensor structure without Sagnac ring, the performance is greatly improved, the maximum sensitivity is up to 234 nm/RIU, and it has good temperature stability. The sensor has the advantages of miniaturization, high integration and high sensitivity, and can be used in industry, chemical detection, agriculture and other fields.

KEYWORDS

photonic crystal fiber, Sagnac ring, refractive index sensor, high birefringence, temperature sensor

Introduction

Optical fiber sensor is different from traditional electrical sensor, the complex mechanical structure is replaced by optical fiber [1–3]. Fiber optic sensors are widely used in strain, temperature, refractive index and other parameters measurement because of their small size, anti-electromagnetic interference and high speed [4–6]. As one of the basic physical parameters, refractive index has important applications in the fields of medicine, biochemistry and life science [7–9]. Optical fiber refractive index sensor is the basis of optical fiber sensor. An excellent fiber refractive index sensor can be extended to other fields of sensing detection. If it is extended to the temperature detection field, only

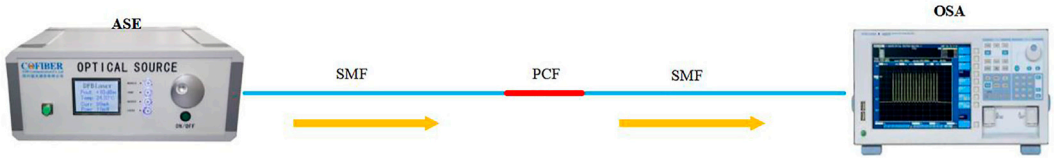

FIGURE 1
Single-mode fiber—PCF- Single-mode fiber structure diagram.

temperature-sensitive materials need to be coated in the sensing area. Extending to the field of humidity detection only requires coating the sensing area with moisture-sensitive material. Therefore, it is very important to propose a kind of fiber refractive index sensor with good performance [10–12].

At present, fiber optic devices used for sensing mainly include fiber Bragg grating, long period grating and Mach-Zehnder interferometer based on special fibers [13–16]. Vanita et al. designed a fiber refractive index sensor with a sensitivity of 197.33nm/RIU through malposition fusion mach-zehnder structure [17], but this structure has the disadvantage of low mechanical strength. In 2021, Zheng et al. proposed three kinds of fiber fusion interference structures, with the sensitivity reaching 101.996 nm/RIU [18]. But it is very difficult to manufacture. Abdul-jabbar et al. designed a fiber refractive index sensor in 2021 based on Fabry-Perot principle, with a sensitivity of 34.338nm/RIU [19]. However, due to the characteristics of the structure, it is greatly affected by temperature. PCF is also a hot topic in optical fiber sensing [20]. But at present, most photonic crystal fiber sensors are only studied in the simulation range [21]. In the research of photonic crystal fiber sensor, the performance of polished PCF sensor is higher than that of ordinary PCF sensor due to its high birefringence [22], but it is difficult to manufacture in practical experiment.

In order to solve the above problems, we put forward a new scheme. In this study, a Sagnac ring was added into the sensing structure of traditional single-mode fiber (SMF) and PCF, and a novel refractive index sensor was fabricated by using the cone-region coupling and the evanescent field superposition effect at the interference region of PCF. The Sagnac ring structure has a high birefringence characteristic even without polishing because the two beams travel in opposite directions and have inconsistent optical paths. The performance of Sagnac combined with PCF was compared with that of conventional SMF-PCF-SMF. The experimental results show that the sensitivity reaches 234.78252 nm/RIU in the refractive index 1.3355-1.3560 range.

Sensor manufacturing and principle analysis

SMF-PCF-SMF structure is a basic refractive index sensor unit that achieves Mach-Zehnder interference principle through fiber core mismatch. The structure is shown in Figure 1. In this paper, the refractive index sensing ability and temperature stability of SMF-PCF-SMF structure were measured first. The experimental device is shown in Figure 1. The two ends of single-mode fiber are respectively connected with broadband light source (ASE) and spectrum analyzer (OSA).

Next, we will remove the coating layer of the single-mode fiber on both sides, and stack them together, and put them into the fiber fusion taper platform. We operate a computer to control the length of the pull-out cone. In the pull-out process, the waveguides of two optical fibers are coupled and the light in one waveguide begins to affect the square distribution of the waveguides in the other fiber. A fused tapered Sagnac ring with a coupling length of 25 mm is formed and the tapered region is encapsulated. The structure of the Sagnac ring is shown in Figure 2, and which shows the instrument and method for manufacturing and testing. After the light signal is emitted by the broadband light source, the beam is evenly divided into two beams of equal intensity from both directions to the PCF by the fused tapered coupler. At this time, PCF and the pull cone area act together to form the sensing unit. Compared to Figure 1, there is an increased phase delay of $\pi/2$ when light passes through the coupler. In addition, due to the structure of PCF, the light source at PCF enters the cladding and produces interference, and the spectrum at this time can be measured by OSA.

Figure 3 shows the simulation results of mode refractive index and electric field distribution of the two parts of the structure used in this paper. Figure 3A part of photonic crystal fiber, Fig in the section for the refractive index of the two models, the red arrow for the direction of the electric field, electric field can be seen from the simulation results, under the condition of without considering manufacture error, we use the PCF structure of the odd and even mode refractive index are the same, there is no double refraction phenomenon. In Figure 3B, it can be seen that the refractive index values of the two modes in the pull-cone coupling part are different, indicating obvious birefringence phenomenon. It can be inferred that the proposed structure should have higher sensitivity than the simple PCF sensor.

Ignoring the insertion loss in the Sagnac ring, the transmittance T of the injected Sagnac interferometer is [23]:

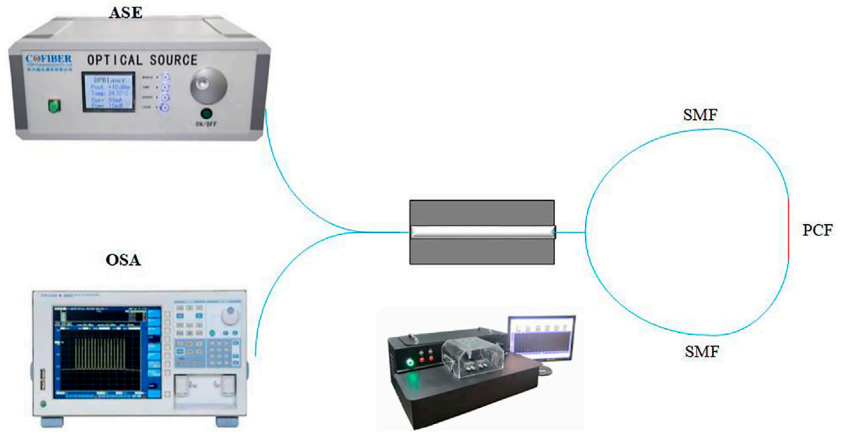

FIGURE 2
Sagnac interferometer sensor structure diagram.

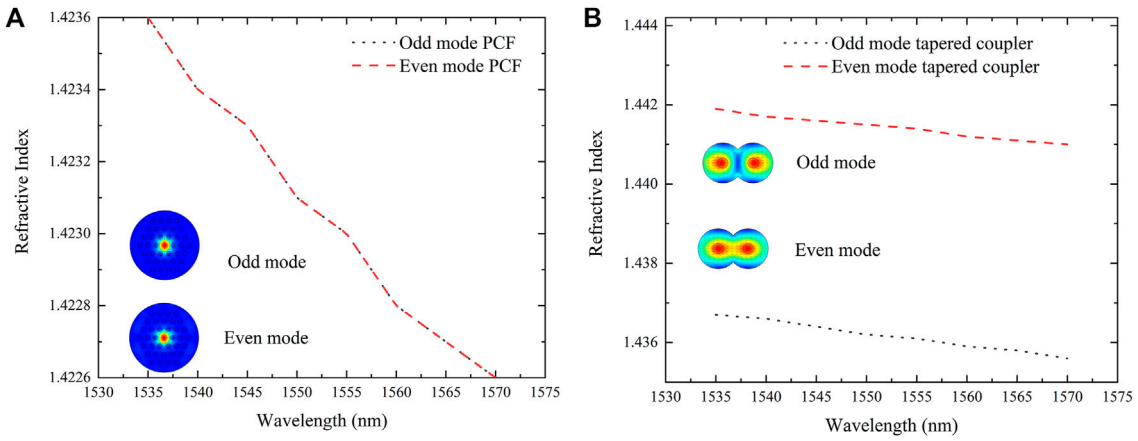

FIGURE 3
Optical fiber mode refractive index simulation and electric field diagram. **(A)** Partial refractive index simulation and electric field diagram of PCF. **(B)** Partial refractive index simulation and electric field diagram of tapered coupler.

$$T = [1 - \cos(\varphi)]/2 \tag{1}$$

In the experimental structure designed by us, light first excites even and odd modes through the cone region. Even mode and odd mode form interference in the coupling region of the taper. Due to the birefringence effect in the coupling region, the superposition of two interference spectra with different polarities and different interference periods can be obtained at the output end. At this point, the phase difference between even mode and odd mode can be expressed as [24]:

$$\varphi_{even} = \frac{2\pi L\left(n^x_{even} - n^y_{even}\right)}{\lambda} \tag{2}$$

$$\varphi_{odd} = \frac{2\pi L\left(n^x_{odd} - n^y_{odd}\right)}{\lambda} \tag{3}$$

Where, L is the length of the draw-cone 25mm, n_{even} and n_{odd} are the effective refractive index of even and odd modes. $B_{even} = n^x_{even} - n^y_{even}$, $B_{odd} = n^x_{odd} - n^y_{odd}$ represents the birefringence coefficients of even mode and odd mode in the waveguide respectively. The λ is the wavelength of incident light. Due to the structural characteristics of Sagnac ring, the two beams propagate in opposite directions, and the phase difference between even mode and odd mode is [25]:

$$\varphi = \frac{2\pi BL}{\lambda} \tag{4}$$

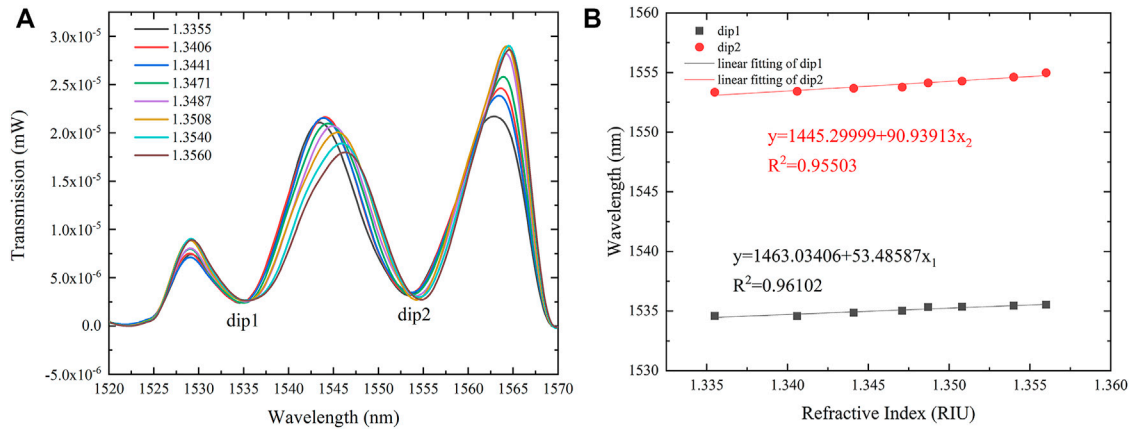

FIGURE 4
SMF-PCF-SMF Index sensor performance diagram. **(A)** Interference spectrum. **(B)** Fitting diagram.

Where, B is the birefringence coefficient, specifically, B = B_{odd}-B_{even}.

When the light beam reaches the mismatch region of PCF core, the light of the core is excited to the cladding layer, and the light in the cladding layer is coupled with the light in the core. When the external environment changes, the optical diameter difference between the cladding transmission light and the fiber core transmission light changes, and the phase difference is [26]:

$$\varphi_{PCF} = \frac{2\pi Z n_{eff}}{\lambda} \quad (5)$$

In this formula, x is the wavelength of the working light wave, Z is the total length of PCF, 20 mm in this paper, neff = N1-N2 is the refractive index of the fiber core, and N2 is the refractive index of the cladding. The total phase difference of the structure in Figure 2 is $\varphi_{all} = \varphi + \varphi_{PCF}$. In this paper, ethanol fusion deionized water (hereafter referred to as solution) was used as the test solution and the temperature stability of the structure in air was analyzed.

Experimental measurement and discussion of refractive index sensor

First of all, we carried out the fusion of single-mode fiber-PCF-single-mode fiber. After the fusion, a basic Machzand structure sensing unit was formed and tested.

We first put the sensor unit into solutions with different refractive indexes at room temperature of 24°C. For the accuracy of the experiment, eight solutions with different concentrations were conFigd for comparison. And after this measurement, the sensor unit is cleaned with deionized water and put into the next solution after drying. As can be seen from Figure 4A, with the increase of refractive index of solution (1.3355-1.3560), the spectrum appeared red-shift. The principle of this structure is the Mach-Zehnder interference caused by core mismatch caused by connecting single mode fiber and photonic crystal fiber. When the refractive index of solution changes, the coupling effect of single-mode fiber and PCF changes. The spectrum drifts. Subsequently, we performed a fitting analysis on dip1 and dip2 in Figure 4B, and it was clear that the sensitivities reached 53.48587nm/RIU and 90.93913nm/RIU, respectively, with R^2 saying 0.96102 and 0.95503. Experimental results show that the sensor using photonic crystal fiber has good refractive index sensitivity. However, when the refractive index of the solution increases further, the spectral shape changes, so we do not analyze the higher refractive index.

Next, we measured the temperature sensitivity of the sensor in the air, and the experimental device was a blast drying oven and a thermometer. In order to ensure the accuracy of measurement, we kept the same temperature for 20 min and then extracted the spectrum. It can be seen from Figure 5A that when the sensor unit detects the temperature in the air, the first trough of the spectrum becomes smaller, while the second trough remains unchanged. When the temperature rises (20–80°C), the wavelength is red-shifted, and we fit the dip. It can be clearly seen from Figure 5B that the temperature sensitivity of the sensing unit is 19.54 p.m./°C, and R^2 is 0.73366. The results show that the sensor is not suitable for temperature sensing, and the temperature sensitivity is far less than the refractive index sensitivity, which shows that the temperature stability of the sensor is very good.

Next, the two sides of single-mode fiber are fused and tapered to form Sagnac structure. The same refractive index and temperature sensing experiments were carried out. It can be seen from Figure 6A that when the refractive index of solution increases, the spectrum also occurs red shift. Different from the above structure, there are two Mach-Zehnder interferences in

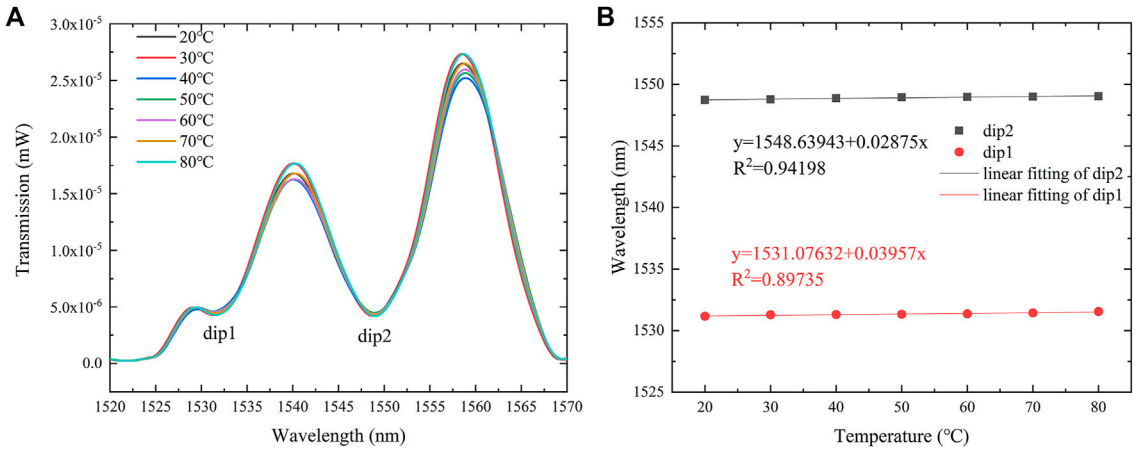

FIGURE 5
SMF-PCF-SMF Temperature sensor performance diagram. **(A)** Interference spectrum. **(B)** Fitting diagram.

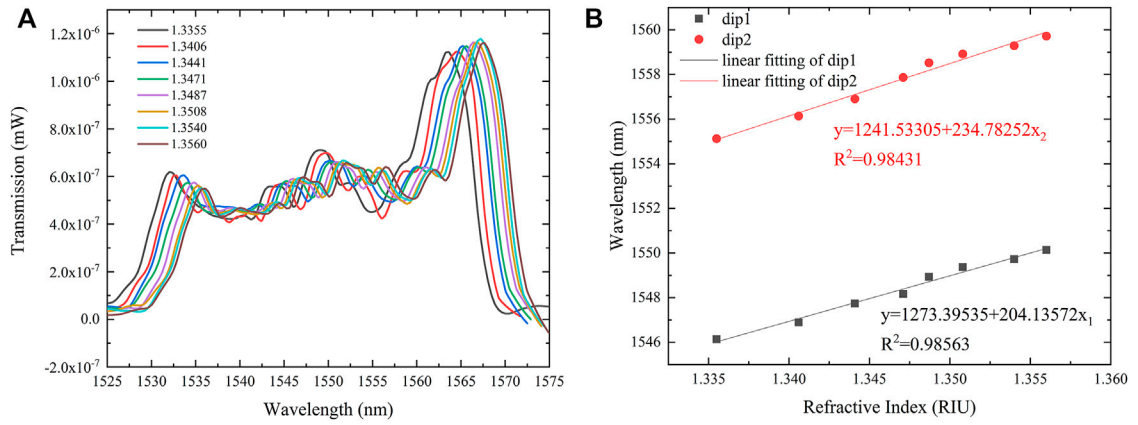

FIGURE 6
Sagnac interference structure refractive index sensor performance diagram. **(A)** Interference spectrum. **(B)** Fitting diagram.

this structure, respectively in the part of the tapered coupler and the part of the single mode and photonic crystal junction. In addition, light is split through the tapered coupler, and there is a certain optical path difference causing the second Mach-Zehnder interference with birefringence effect. Dip1 and dip2 are relatively obvious regions where wavelength drift can be distinguished. And it has good linearity. The peak on the side can also be used. In fact, there is little difference in sensitivity, but there is some deformation near the peak of high wavelength, so it is not possible to accurately judge which one is the correct peak. Dip is chosen for all. The fitting analysis of dip1 and dip2 shows that the refractive index sensitivity reaches 204.13572 nm/RIU and 234.78252 nm/RIU, respectively, which increases significantly compared to the sensor structure without Sagnac. And R^2 reached 0.98563 and 0.98431, respectively, proving that Sagnac structure of the sensor performance is superior.

Figure 7 shows the temperature sensing performance of Sagnac structure. It can be seen that when the object to be measured is room temperature, the spectrum becomes smooth. As the temperature rises, the spectrum also appears red shift, but the displacement amplitude is smaller than that of Sagnac free structure, which is contrary to the case of refractive index sensor. Through our analysis, this is because when the Sagnac ring is formed, the internal loss of the structure increases. Therefore, although the refractive

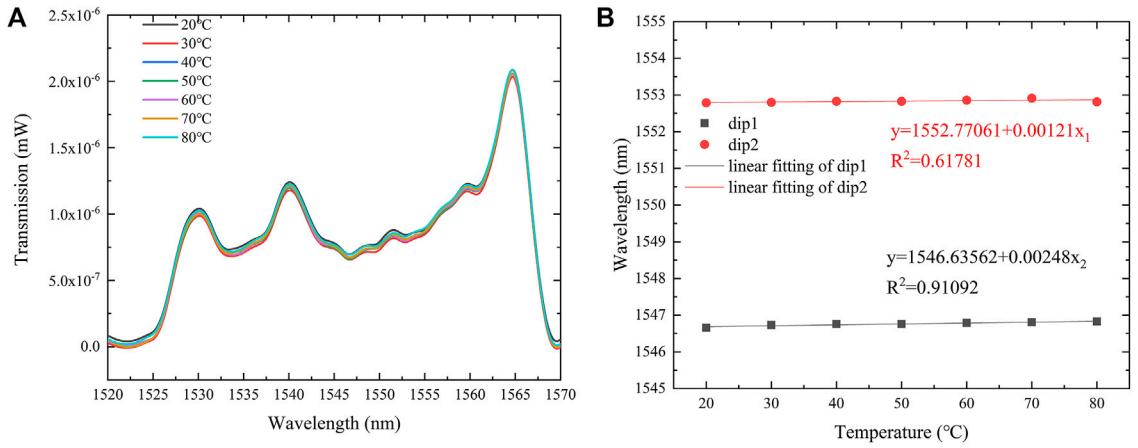

FIGURE 7
Temperature sensing performance diagram of Sagnac interference structure. **(A)** Interference spectrum. **(B)** Fitting diagram.

TABLE 1 Compared with the experimental data of optical fiber sensor published in recent years.

Structure	Sensing range	Sensing performance (nm/RIU)	Temperature deviation (pm/°C)	Year of publication
No core fiber	1.33–1.38	197.33	N/A	2017 [16]
Three kinds of fiber	1.3333–1.3794	101.996	4.9	2021 [18]
Fabry-Perot	1.3436–1.3481	34.338	N/A	2021 [19]
Polarization-maintaining fiber	1.3426–1.3492	48.3	N/A	2015 [27]
Dislocation PCF	1.339–1.347	169.63928	N/A	2021 [28]
Our work	1.3355–1.3560	234.78252	2.48	

index sensitivity increases, the temperature sensitivity with smaller change decreases due to the loss. Figure 7B shows that the temperature sensitivity of Sagnac structure is 2.48 p.m./°C and 1.21 p.m./°C, and R^2 is 0.91092 and 0.61781, respectively. The experimental results show that the structure is not suitable for temperature sensing because of its weak temperature sensing. It is also proved that the structure has high temperature stability.

As can be seen from the comparison in Table 1, the refractive index sensing ability of the sensor structure designed by us is better than that of some other optical fiber sensors published in recent years within similar sensing range, and is less affected by temperature. We selected and compared the experimental papers published in recent years, and the difficulty of the process is similar to this experiment. Some are difficult to verify by repeated experiments, require very high technological level and pure simulation sensors are not in the range of comparison. The structure is also less difficult to make. In general, it can be regarded as excellent among the experimental fiber sensor papers published in recent years.

Conclusion

This paper presents a PCF refractive index sensor with Sagnac ring structure. Through simulation analysis, it is proved that the structure has high birefringence effect and strong evanescent field, and it is speculated that it has higher sensing ability. We experimentally analyzed the sensitivity and temperature stability of refractive index measurement, and compared it with Single-Mode Fiber-PCF-Single-Mode Fiber. Experimental results show that Sagnac ring structure can enhance the refractive index sensitivity and reduce the influence of temperature on the sensor. The maximum refractive index sensitivity was 234.78252 nm/RIU in the refractive index range 1.3355–1.3560.

Data availability statement

The original contributions presented in the study are included in the article/supplementary material, further inquiries can be directed to the corresponding author.

Author contributions

Conceptualization, ZL and HL; methodology, ZZ; validation, ZL and ZZ; formal analysis, ZZ; investigation, ZL and ZZ; resources, ZL; data curation, ZZ; writing—original draft preparation, ZZ; writing—review and editing, ZL; visualization, HL; supervision, ZL; project administration, ZL; funding acquisition, ZL All authors have read and agreed to the published version of the manuscript.

Funding

This work was supported by the National Natural Science Foundation of China (grant number 52102164).

Conflict of interest

The authors declare that the research was conducted in the absence of any commercial or financial relationships that could be construed as a potential conflict of interest.

Publisher's note

References

1. Li L, Wang Z, Ma Q, Wang M, Wu Q, Chen H, et al. Sagnac ring humidity sensor with a melting cone based on graphene properties. *IEEE Sens J* (2021) 21(14), 16061–5. doi:10.1109/jsen.2021.3075443

2. Barnes J, Li S, Goyal A, Abolmaesumi P, Mousavi P, Lock HP. Broadband vibration detection in tissue phantoms using a fiber fabry-perot cavity. *IEEE Trans Biomed Eng* (2018) 65(4):921–7. doi:10.1109/tbme.2017.2731663

3. Zhang Z, Zhang F, Xu B, Xie H, Fu B, Lu X, et al. High-sensitivity gas detection with air-lasing-assisted coherent Raman spectroscopy. *Ultrafast Sci* (2022) 2022: 1–8. doi:10.34133/2022/9761458

4. Li X, Zhang H, Qian C, Ou Y, Shen R, Xiao H. A new type of structure of optical fiber pressure sensor based on polarization modulation. *Opt Lasers Eng* (2020) 130: 106095. doi:10.1016/j.optlaseng.2020.106095

5. Chen Y, Wan H, Chen Q, Zhou Q, Zhang Z. High sensitivity optical fiber temperature sensor based on rare-earth-doped double-fiber peanut. 中国激光 (2020) 47:0110001. doi:10.3788/cjl202047.0110001

6. Pathak AK, Rahman ABM, Singh VK, Kumari S. Sensitivity enhancement of a concave shaped optical fiber refractive index sensor covered with multiple Au nanowires. *Sensors* (2019) 19(19):4210. doi:10.3390/s19194210

7. Eryurek M, Karadag Y, Ghafoor M, Bavili N, Cicek K, Kiraz A. Liquid refractometric sensors based on optical fiber resonators. *Sensors Actuators A: Phys* (2017) 265:161–7. doi:10.1016/j.sna.2017.08.019

8. Fan X, White IM, Shopova SI, Zhu H, Suter JD, Sun Y. Sensitive optical biosensors for unlabeled targets: A review. *Analytica Chim Acta* (2009) 620(1-2): 8–26. doi:10.1016/j.aca.2008.05.022

9. Baldini F, Brenci M, Chiavaioli F, Giannetti A, Trono C. Optical fibre gratings as tools for chemical and biochemical sensing. *Anal Bioanal Chem* (2012) 402(1): 109–16. doi:10.1007/s00216-011-5492-3

10. Duan L, Yang X, Lu Y, Yao J. Hollow-fiber-based surface plasmon resonance sensor with large refractive index detection range and high linearity. *Appl Opt* (2017) 56:9907–12. doi:10.1364/ao.56.009907

11. Gao X, Ning T, Zhang C, Xu J, Zheng J, Lin H, et al. A dual-parameter fiber sensor based on few-mode fiber and fiber Bragg grating for strain and temperature sensing. *Opt Commun* (2020) 454:124441. doi:10.1016/j.optcom.2019.124441

12. Fu Y, Cao J, Yamanouchi K, Xu H. Air-Laser-based standoff coherent Raman spectrometer. *Ultrafast Sci* (2022) 2022:1–9. doi:10.34133/2022/9867028

13. Ma YF, Feng W, Qiao SD, Zhao ZX, Gao SF, Wang YY. Hollow-core anti-resonant fiber based light-induced thermoelastic spectroscopy for gas sensing. *Opt Express* (2022) 30(11):18836–44. doi:10.1364/oe.460134

14. Polito D, Arturo Caponero M, Polimadei A, Saccomandi P, Massaroni C, Silvestri S, et al. A needle-like probe for temperature monitoring during laser ablation based on FBG: Manufacturing and characterization. *J Med Devices* (2015) 9(4):1590–4.

15. Poletti F, Petrovich MN, Richardson DJ. Hollow-core photonic bandgap fibers: Technology and applications. *Nanophotonics* (2013) 2:315–40. doi:10.1515/nanoph-2013-0042

16. Bhardwaj V, Kishor K, Vinod Kumar S. Experimental and theoretical analysis of connector offset optical fiber refractive index sensor. *Plasmonics* (2017) 12(6): 1999. doi:10.1007/s11468-016-0473-1

17. Qiao SD, Sampaolo A, Patimisco P, Spagnolo V, Ma YF. Ultra-highly sensitive HCl-LITES sensor based on a low-frequency quartz tuning fork and a fiber-coupled multi-pass cell. *Photoacoustics* (2022) 27:100381. doi:10.1016/j.pacs.2022.100381

18. Yuanyuan Z, Xiaozhan Y, Wenlin F, Wei F. Optical fiber refractive index sensor based on SMF-TCF-NCF-SMF interference structure. *Optik - Int J Light Electron Opt* (2021) 226:165900. doi:10.1016/j.ijleo.2020.165900

19. Nisreen A-J, Kadhim Shehab A, Naseef Intisar A. Characterization study of optical fiber refractive index sensor based on fabry-perot interferometer. *J Phys Conf Ser* (2021) 1963:1. doi:10.1088/1742-6596/1963/1/012052

20. Liu C, Su W, Wang F, Li X, Yang L, Sun T, et al. Theoretical assessment of a highly sensitive photonic crystal fibre based on surface plasmon resonance sensor operating in the near-infrared wavelength. *J Mod Opt* (2018) 66:1–6. doi:10.1080/09500340.2018.1508776

21. Zhang S, Li J, Li S. Design and numerical analysis of a novel dual-polarized refractive index sensor based on D-shaped photonic crystal fiber. *Metrologia* (2018) 55:828–39. doi:10.1088/1681-7575/aae757

22. Zhang ZW, Shen T, Wu HB, Feng Y, Wang X. Polished photonic crystal fiber refractive index sensor based on surface plasmon resonance. *J Opt Soc Am B* (2021) 38(12):F61–F68. doi:10.1364/josab.433726

23. Li X. G., Nguyen L. V., Zhao Y., Ebendorff-Heidepriem H., Warren-Smith S. C. High-sensitivity Sagnac-interferometer biosensor based on exposed core microstructured optical fiber. *Sensors Actuators B Chem[J]* (2018) 269:103–109. doi:10.1016/j.snb.2018.04.165

24. Hao JQ, Han BC. Highly sensitive tapered optical fiber coupler-based gas refractive index sensor enhanced by the Vernier effect. *Opt. Eng.* (2020) 59 (6): 066102. doi:10.1117/1.OE.59.6.066102

25. Yang F, Wu Y.J, Shi J, Yang K, Xu W, Guo C.J, et al. Curvature sensor based on fiber ring laser with Sagnac loop. *Opt Fiber Tech* (2020) 60:102341. doi:10.1016/j.yofte.2020.102341

26. Liu Q, Li S-G, Chen H. Enhanced sensitivity of temperature sensor by a PCF with a defect core based on Sagnac interferometer. *Sensors and Actuators B: Chemical[J]* (2018) 254. doi:10.1016/j.snb.2017.07.120

27. Zeng H, Shen C, Lu Y, Liu H, Dong X, Li C. Refractive index sensor based on polarization maintaining fiber Machzand interference combined with fiber Bragg grating [J]. *Chin J sensors actuators* (2015) 28(11):1727–31.

28. Gao P, Zheng X, Liu Y, Wang Z. *J Shenyang Normal Univ (Natural Science)* (2021) 39(06):506–10.